Supplementary information

Shape Memory Hydrogel with Remodelable Permanent Shapes and Programmable Cold-Induced Shape Recovery Behavior

Xinjun Wu[1], Xin Guan[1], Shushu Chen[1], Jiangpeng Jia[1], Chongyi Chen[1], Jiawei Zhang[2,*] and Chuanzhuang Zhao[1,*]

[a]Mr. X. Wu, Ms. X. Guan, Ms. S. Chen, Mr. J. Jia, Prof. Dr. C. Chen, Prof. Dr. C. Zhao, School of Materials Science & Chemical Engineering, Key Laboratory of Impact and Safety Engineering, Ministry of Education, Ningbo University, Ningbo, Zhejiang 315211, China,

*__Corresponding author__. E-mail: zhaochuanzhuang@nbu.edu.cn

[b]Prof. Dr. J. Zhang, School of Material Science and Engineering, Tiangong University, Tianjin 300387, China,

*__Corresponding author__. E-mail: zhangjiawei@tiangong.edu.cn

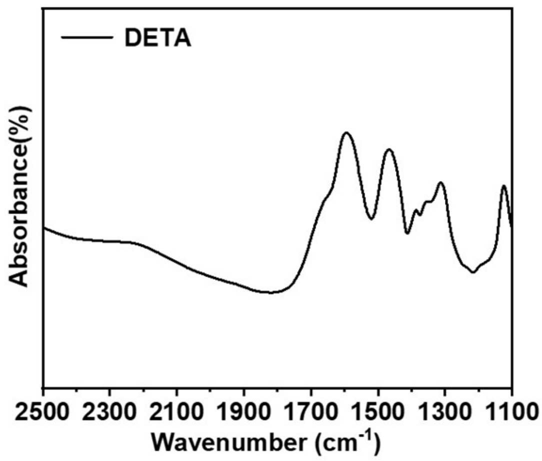

Fig. S1. FTIR spectrum of DETA.

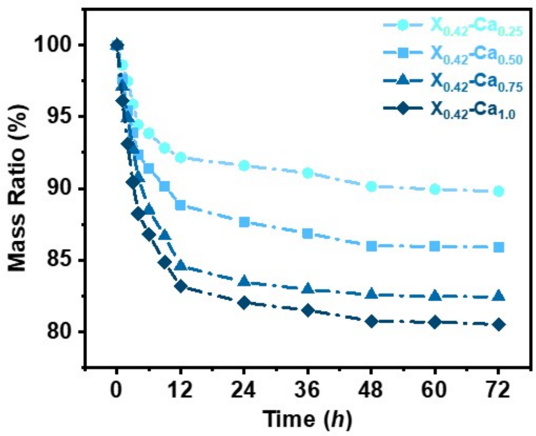

Fig. S2. Mass change curve of PAA/DETA hydrogels during immersing in calcium acetate solution over 72 h. Calcium acetate solutions (0.25 M, 0.5 M, 0.75 M,1 M) were used.

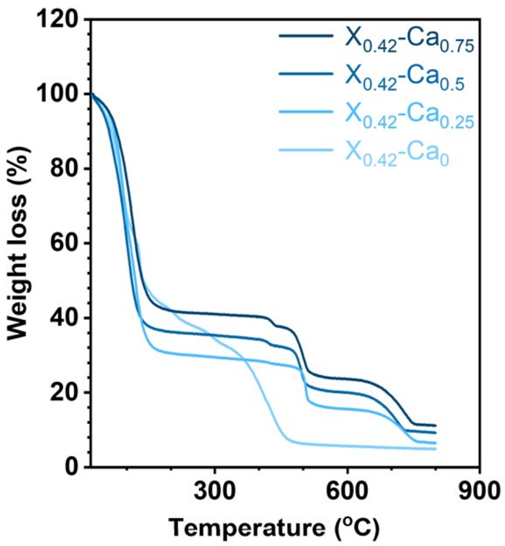

Fig. S3. TGA thermograms of 2CH-gel with 0.42 M of DETA and with different $Ca(Ac)_2$ concentration.

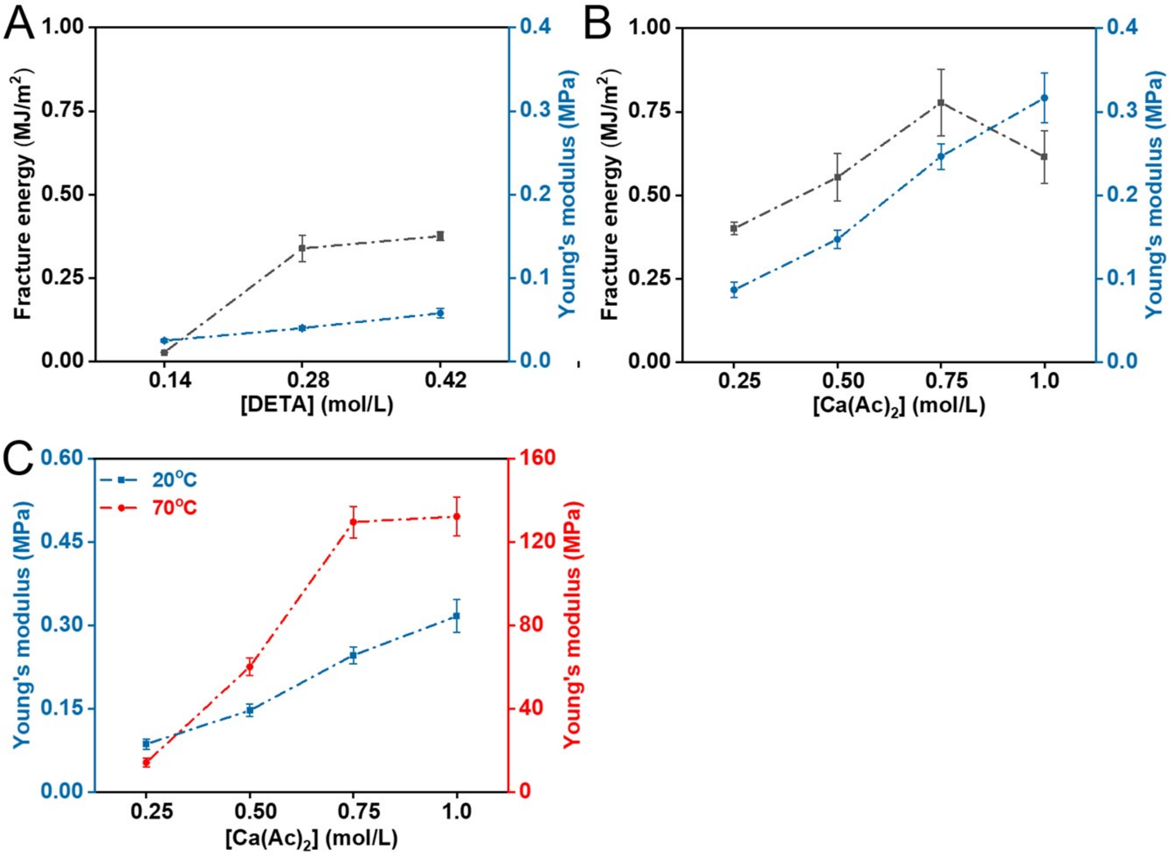

Fig. S4. Comparison of mechanical properties of 2CH-gel. (A) Comparison of fracture energy and modulus of PAA/DETA at different DETA concentrations at 20°C. (B) Comparison of fracture energy and modulus of PAA/DETA at different calcium acetate concentrations at 20°C. The concentration of DETA concentration is 0.42 M. (C) Comparison of the modulus of PAA/DETA at 20°C and 70°C with different calcium acetate concentrations. The concentration of DETA is 0.42 M.

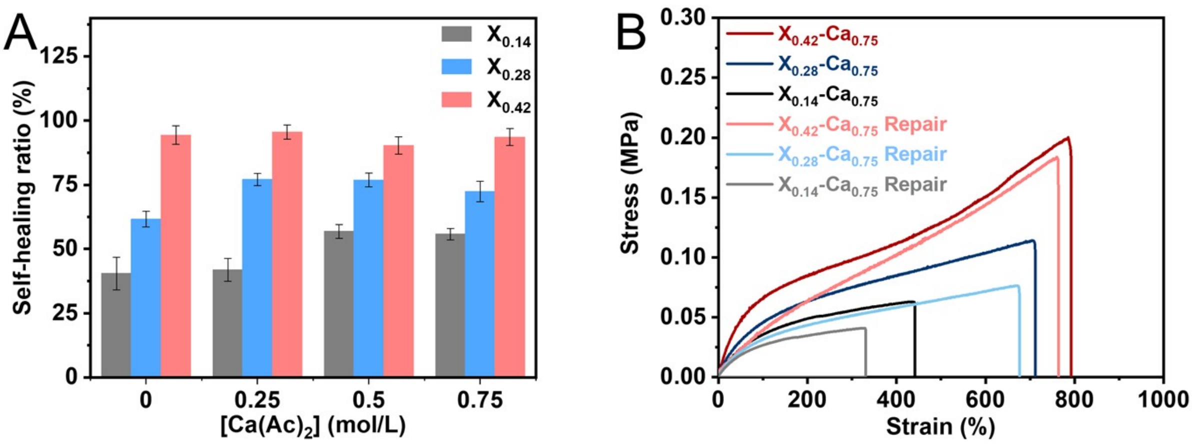

Fig. S5. Self-healing properties of 2CH-gel. (A) The self-healing efficiency of 2CH-gel with different concentration of DETA and $Ca(Ac)_2$. (B) tensile curves of 2CH-gel before and after self-healing.

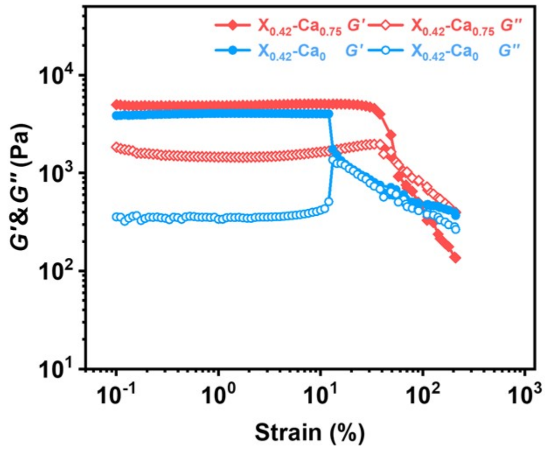

Fig. S6. Oscillatory amplitude sweep of 2CH-gel with and without $Ca(Ac)_2$.

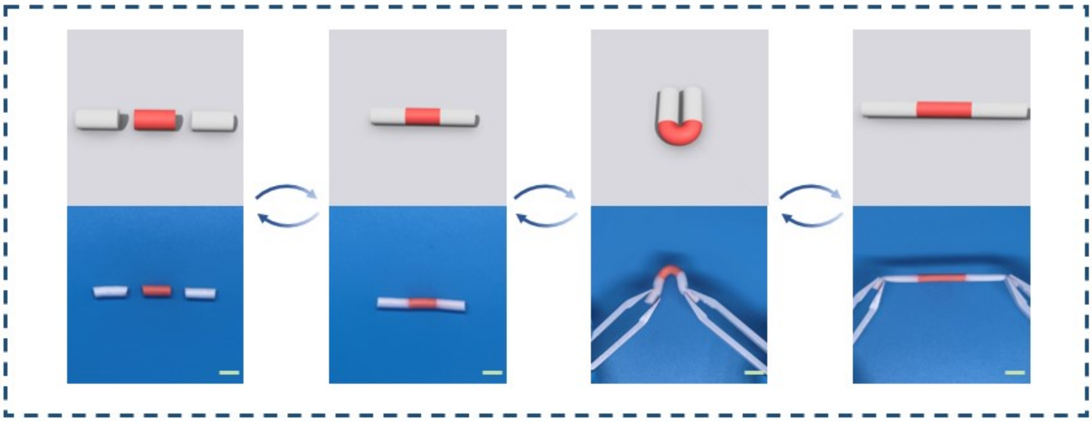

Fig. S7. Photos showing the self-healing performance of 2CH-gel. The 2CH-gel is broken into 3 sections by external force, and the 3 sections are placed together in a humid environment and can repair themselves with only 10 seconds of gentle pressure, the middle hydrogel is stained with eosin to make the display effect more obvious. Scale bars = 1.0 cm.

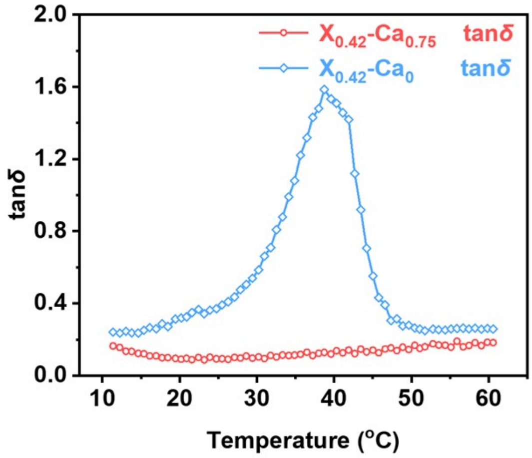

Fig. S8. Loss tangent as function of temperature of 2CH-gel with and without $Ca(Ac)_2$.

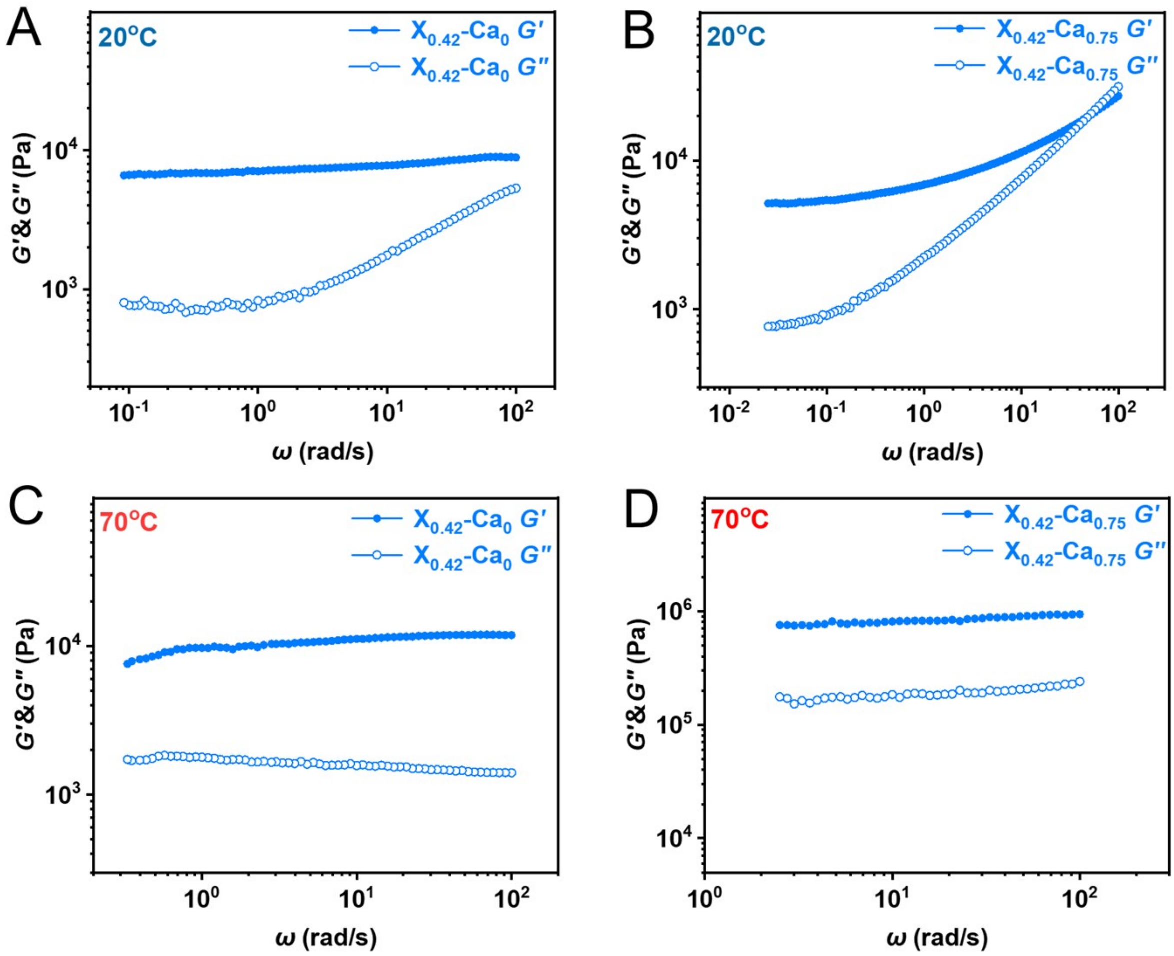

Fig. S9. Angular frequency sweeps of 2CH-gel at different temperatures. (A) Storage modulus and loss modulus of $X_{0.42}$-Ca_0 at 20℃. (B) Storage modulus and loss modulus of $X_{0.42}$-$Ca_{0.75}$ at 20℃. (C) Storage modulus (G') and loss modulus (G'') of $X_{0.42}$-Ca_0 at 70℃. (D) Storage modulus and loss modulus of $X_{0.42}$-$Ca_{0.75}$ at 70℃. All experimental strains were 0.05%.

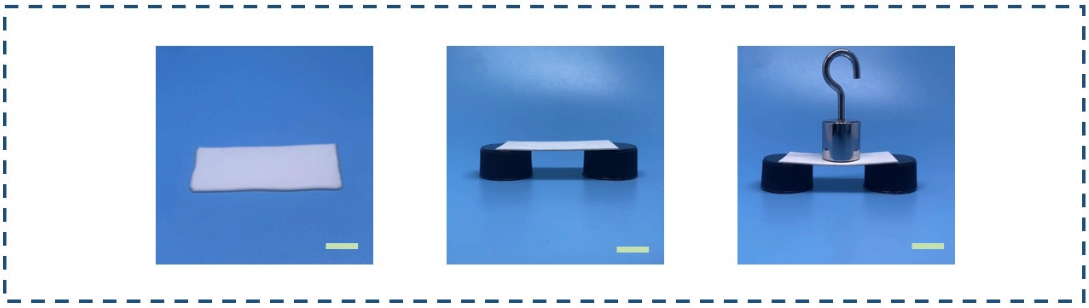

Fig. S10. Photos showing the thermal stiffening effect of 2CH-gel. A piece of 2CH-gel was heated in hot water at 70°C for 10 s, and then it could support a 100 g weight without deformation. (Sample size: ~20 mm ×60 mm × 1 mm). Scale bars = 1.0 cm.

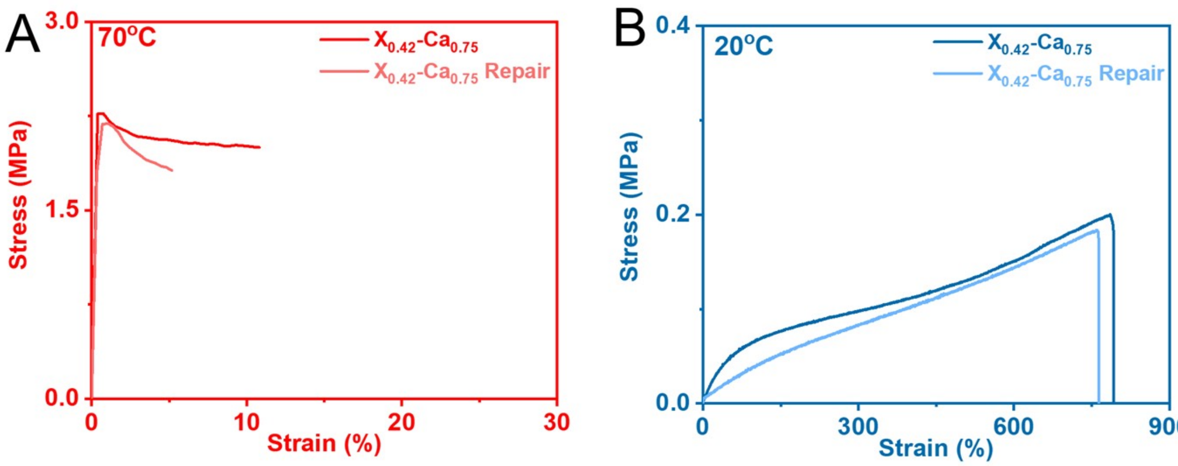

Fig. S11. Stress-strain curves of $X_{0.42}$-Ca_0 and $X_{0.42}$-$Ca_{0.75}$ before and after self-healingat 20 °C and 70 °C.

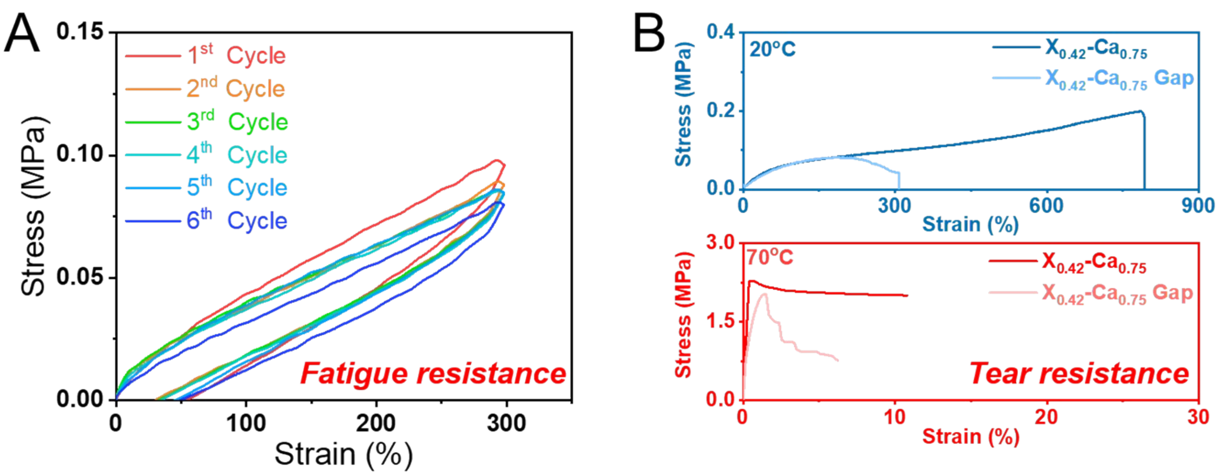

Fig. S12. (A) Fatigue resistance of $X_{0.42}$-$Ca_{0.75}$. (B) Tear resistance of $X_{0.42}$-$Ca_{0.75}$.

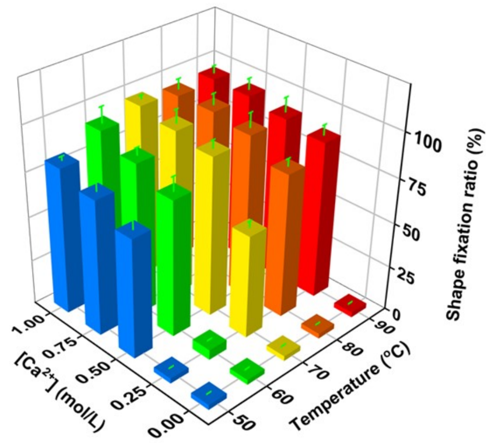

Fig. S13. The influences of the temperature and concentration of $Ca(Ac)_2$ aqueous solution on the shape fixity ratio of 2CH-gel.

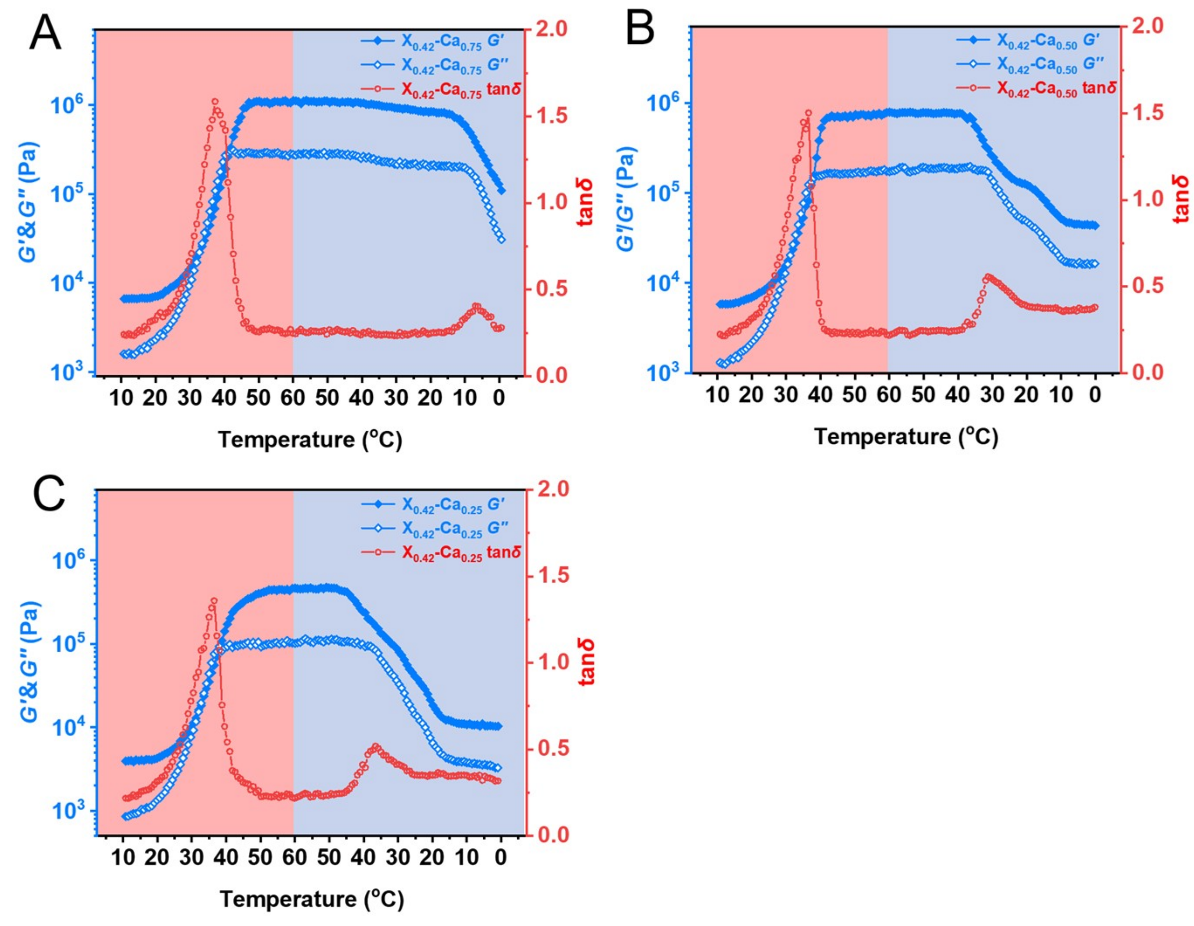

Fig. S14. Storage modulus (G') and loss modulus (G'') of 2CH-gel as a function of temperature. (A) Storage modulus (G') and loss modulus (G'') of $X_{0.42}$-$Ca_{0.75}$ as a function of temperature. (B) Storage modulus (G') and loss modulus (G'') of $X_{0.42}$-$Ca_{0.50}$ as a function of temperature. (C) Storage modulus (G') and loss modulus (G'') of $X_{0.42}$-$Ca_{0.25}$ as a function of temperature.

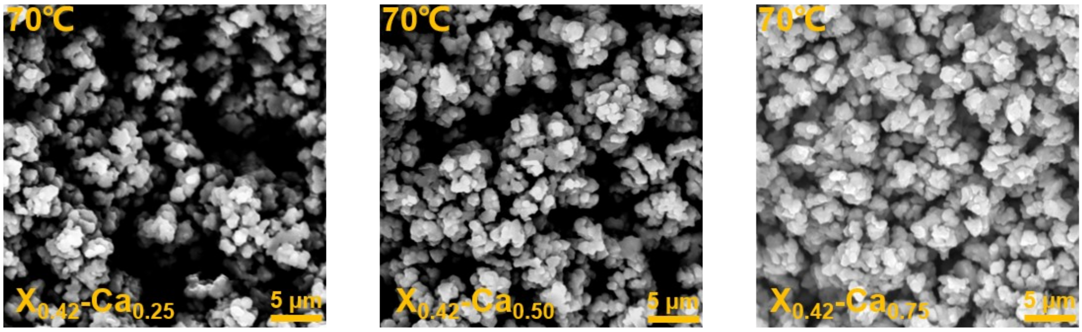

Fig. S15. Scanning electron micrographs of $X_{0.42}$-$Ca_{0.75}$, $X_{0.42}$-$Ca_{0.75}$ and $X_{0.42}$-$Ca_{0.75}$ at 70°C.

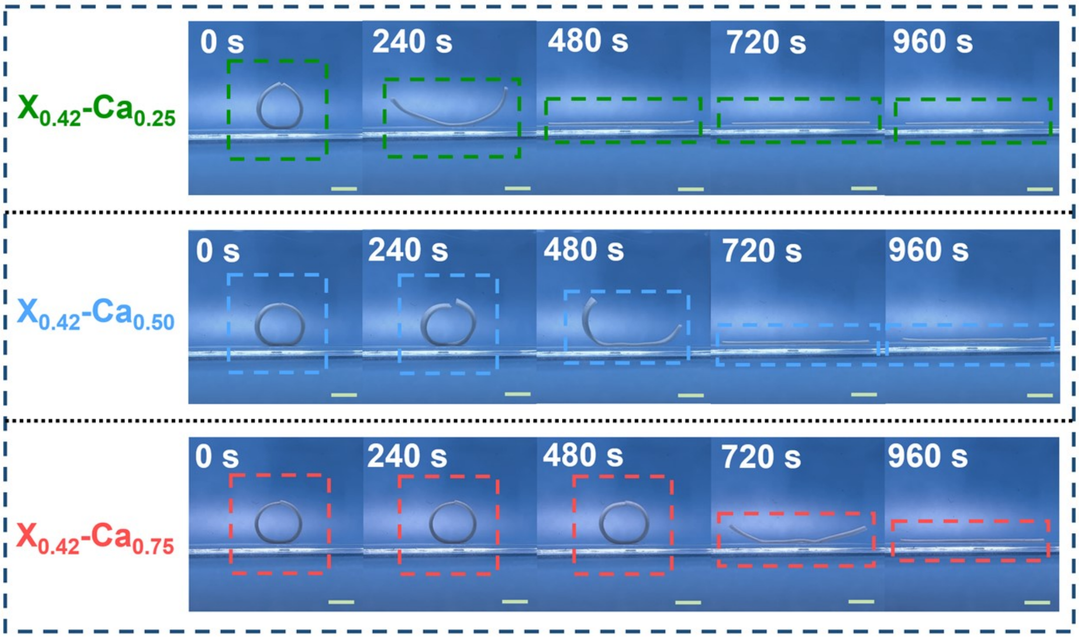

Fig. S16. Photos showing the shape recovery of $X_{0.42}$-$C_{a0.25}$, $X_{0.42}$-$C_{a0.50}$, and $X_{0.42}$-$C_{a0.75}$ after shape fixation in 70 °C water for 10 s.

Fig. S17. 3D message encryption display of 2CH-gel. $X_{0.42}$-$Ca_{0.50}$ and $X_{0.42}$-$Ca_{0.75}$ hydrogels are assembled into a star-shape, letters are printed on each corner and the star-shaped hydrogel are fixed into a tetrahedron by heating at 70°C. Each corner has a different opening speed to display information (left), while the star-shaped hydrogel can be re-assembled to display different information (right). Scale bars = 1.0 cm.

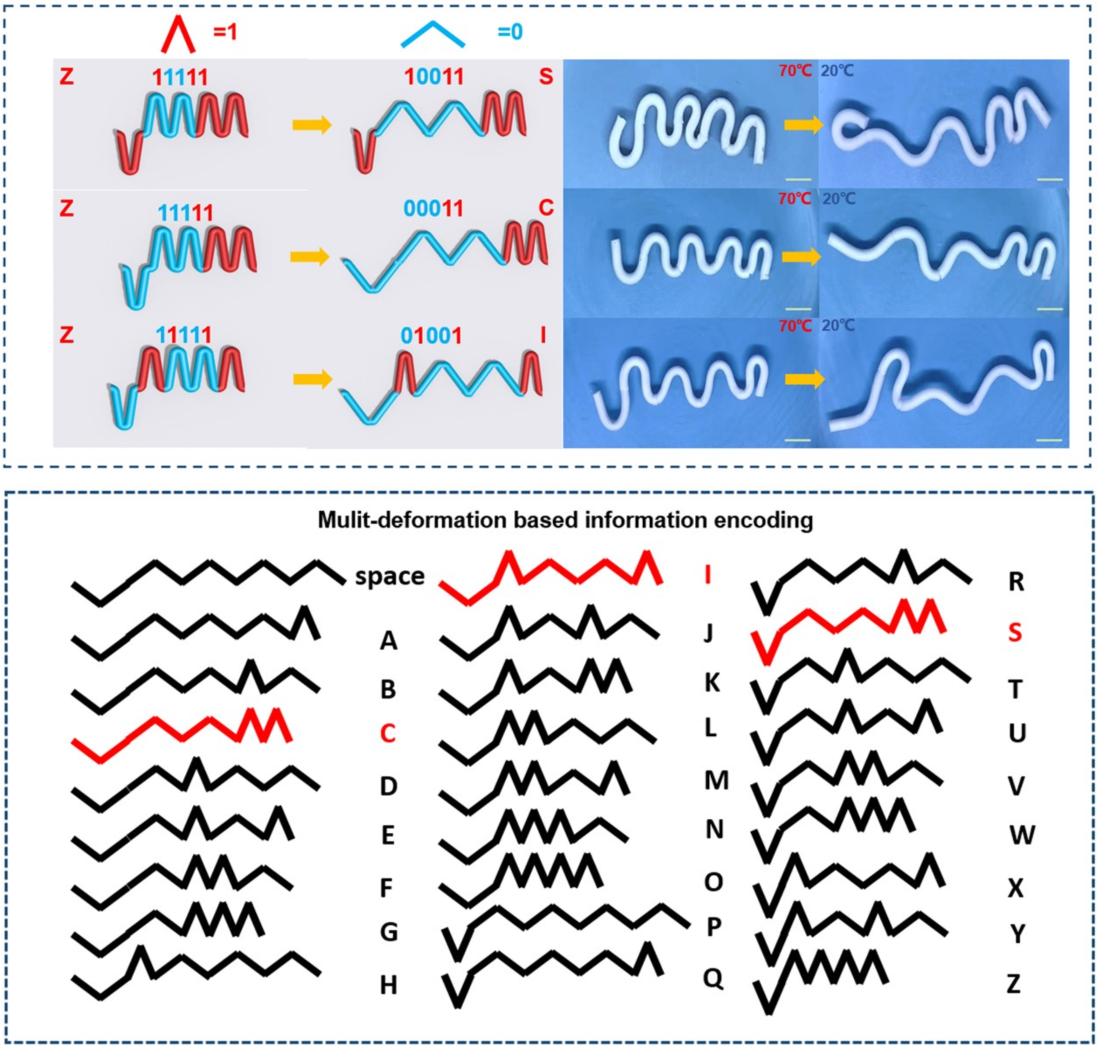

Fig. S18. Schematic illustration and photos showing the information encryption and decryption of 2CH-gel based on the editable shape memory function. $X_{0.42}$-$Ca_{0.50}$ and $X_{0.42}$-$Ca_{0.75}$ hydrogel strips were put together in different sequences, then the hydrogel strip was fixed into specific shapes at 70°C, and the hydrogel could display different messages due to the different softening times of each hydrogel pieces. Scale bars = 1.0 cm.

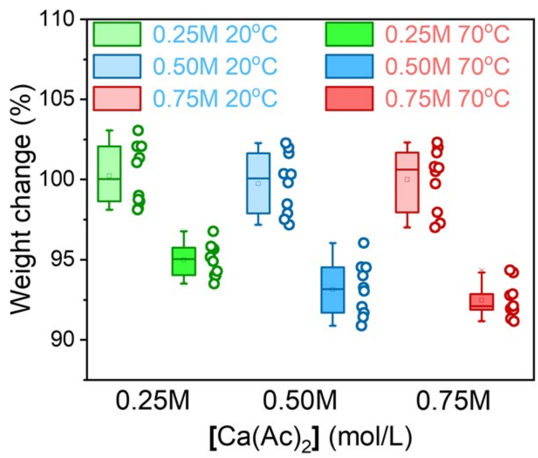

Fig. S19. Weight change before (20°C) and after (70°C) phase separation, sample numbers n = 10.

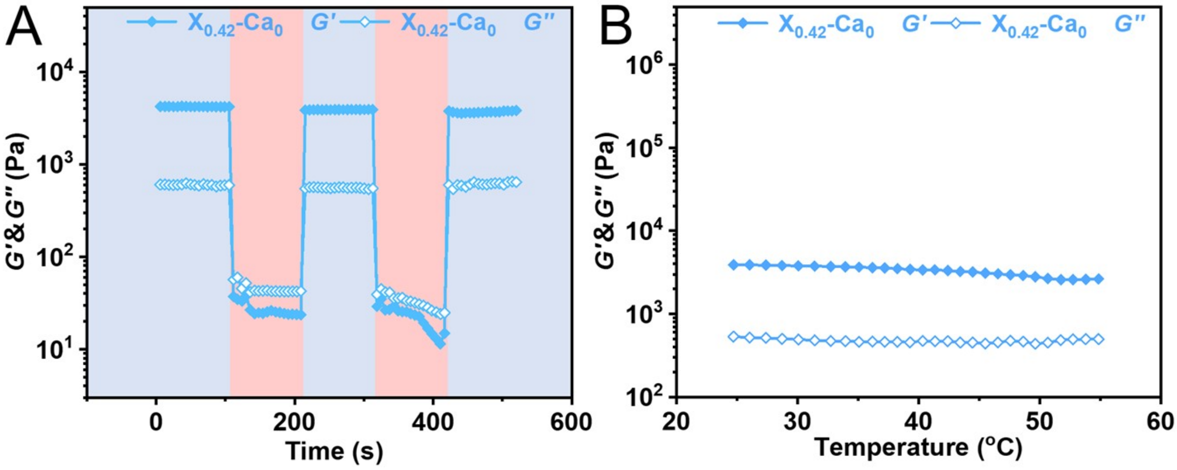

Fig. S20. (A) Alternating strain rheology curves (high strain (250%) and low strain (1.0%)) of 2CH-gel without $Ca(Ac)_2$ after being remodeled. (B) Temperature scanning rheology curves of 2CH-gel without $Ca(Ac)_2$ after being remodeled.

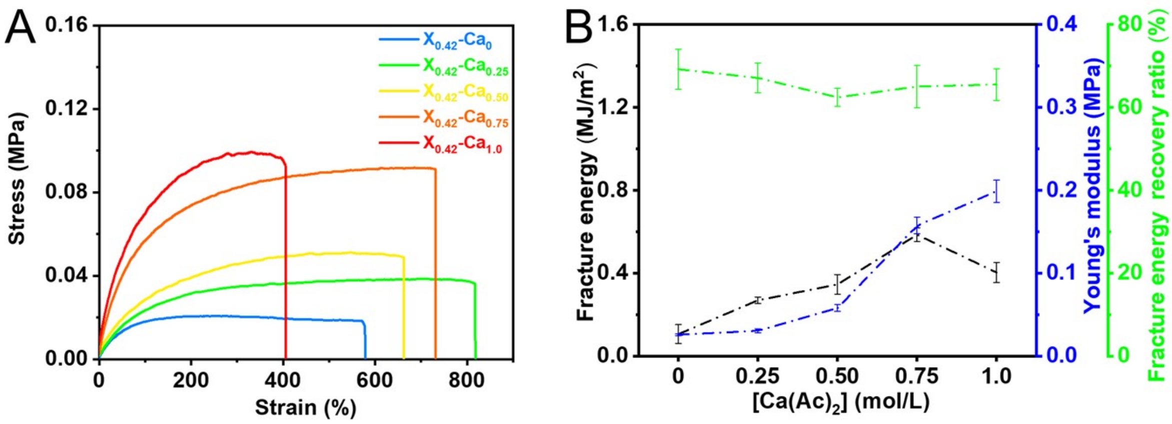

Fig. S21. (A) Tensile curves of 2CH-gel after remodeling. (B) The Young's modulus, fracture energy, and fracture energy recovery rate of 2CH-gel after remodeling.

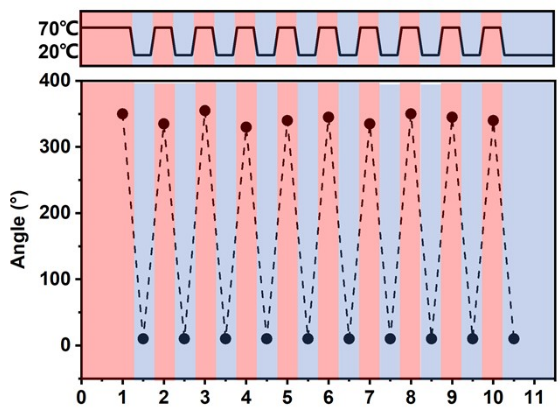

Fig. S22. Cyclic testing indicates the reversible phase separation behavior exhibited by 2CH-gel after remodeling.

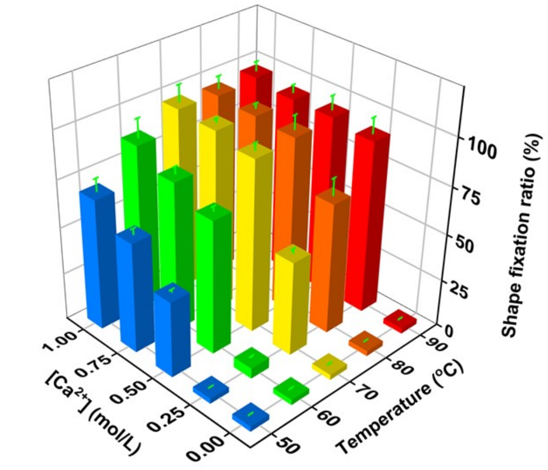

Fig. S23. The influences of the temperature and concentration of $Ca(Ac)_2$ aqueous solution on the shape fixity ratio of 2CH-gel after remodeling.

Table S1. Compositions for 2CH-gel in this work.

Entry	Sample	AAc (mol L^{-1})	DETA (mol L^{-1})	$Ca(Ac)_2$ (mol L^{-1})
1	X_0-Ca_0	3.5	0	0
2	$X_{0.14}$-Ca_0	3.5	0.14	0
3	$X_{0.28}$-Ca_0	3.5	0.28	0
4	$X_{0.42}$-Ca_0	3.5	0.42	0
5	$X_{1.2}$-Ca_0	3.5	1.2	0
6	$X_{0.42}$-$Ca_{0.25}$	3.5	0.42	0.25
7	$X_{0.42}$-$Ca_{0.50}$	3.5	0.42	0.50
8	$X_{0.42}$-$Ca_{0.75}$	3.5	0.42	0.75
9	$X_{0.42}$-$Ca_{1.0}$	3.5	0.42	1.0
10	$X_{0.14}$-$Ca_{0.75}$	3.5	0.14	0.75
11	$X_{0.28}$-$Ca_{0.75}$	3.5	0.28	0.75

Table S2. Comparison of mechanical properties before and after remodeling of $X_{0.42}$-$Ca_{0.75}$ at 70 °C.

$X_{0.42}$-$Ca_{0.75}$	Original state	Remodeled state	Recyle efficiency (%)
Thermal hardening fracture energy (MJ/m^2)	0.220	0.0687	31.2
Thermal hardening young's modulus (MPa)	130	104	80.5
Thermal hardening breaking elongation (%)	10.8	5.72	52.9

Table S3. Comparison of mechanical properties before and after remodeling of $X_{0.42}$-$Ca_{0.75}$ at 20 °C.

$X_{0.42}$-$Ca_{0.75}$	Original state	Remodeled state	Recyle efficiency (%)
Fracture energy (MJ/m^2)	0.913	0.567	62.1
Young's modulus (MPa)	0.157	0.0942	59.8
Breaking elongation (%)	792	731	92.3